Supporting Information

Construction of cross-scale hierarchical ordered Biomimetic architectures enabled by a fluid shear field-assisted sacrificial template method

Yaning Wei, Weicheng Gao, Qianyu Wei, Haoyue Guo, Luyao Wang, Zewen Jiao, Xubo Yuan*, Jin Zhao*

Figure S1. Schematic diagram of the experimental setup (see supplementary video for operation video).

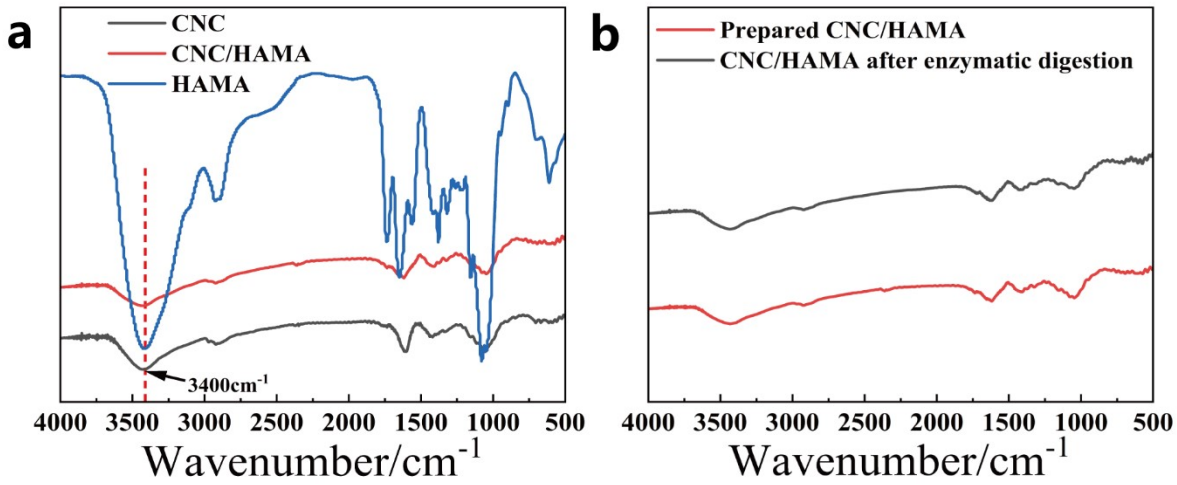

Figure S2. (a) FT-IR spectroscopy of CNC, CNC/HAMA and HAMA. (b) FT-IR spectroscopy of prepared CNC/HAMA and CNC/HAMA after enzymatic digestion.

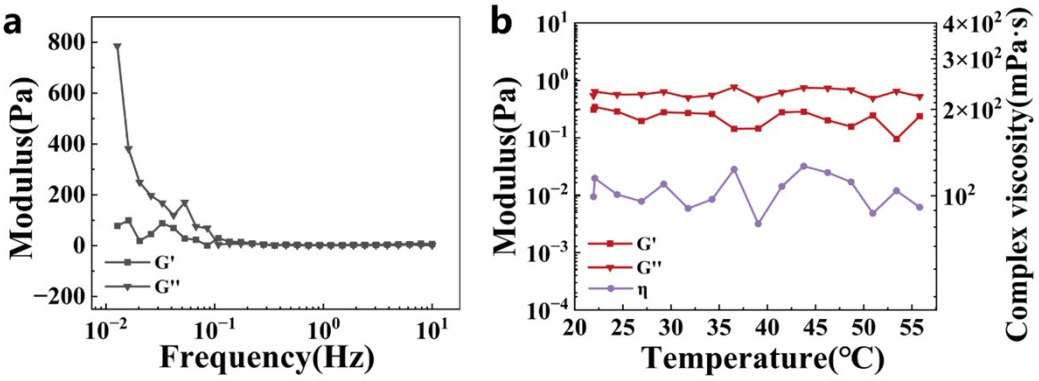

Figure S3. Rheological tests of GelMA bioink: (a) frequency sweep; (b) changes in modulus and complex viscosity of the ink during the temperature range of 20-55 °C.

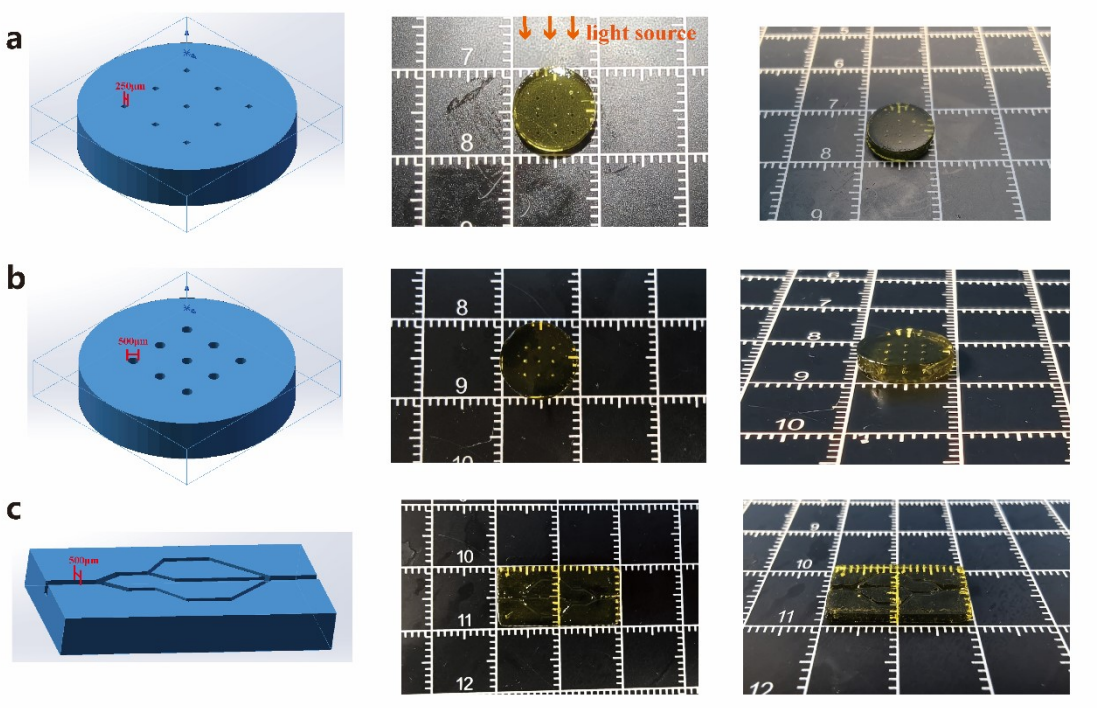

Figure S4. DLP-printed models and their physical top views and front views: (a, b) a cylindrical structure with holes, which has a diameter of 10 mm and a height of 2 mm; (c) a one-to-five flow channel structure.

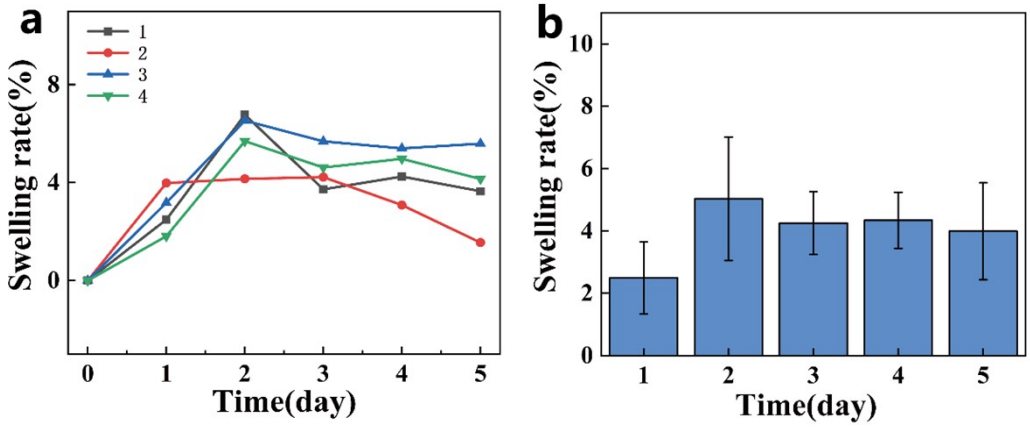

Figure S5. (a) Swelling ratio curves for 5 days for CNC/HAMA hydrogels and (b) their error bars.

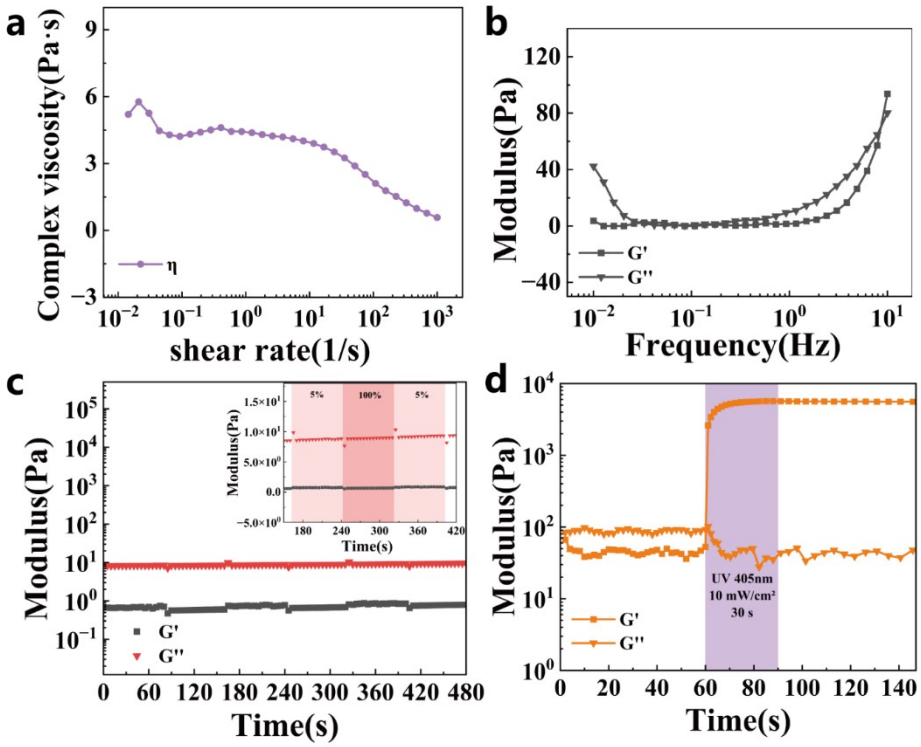

Figure S6. Rheological measurements of CNC/HAMA bioink. (a) Variation of complex viscosity at different shear rates. (b) Variation of modulus at different frequencies. (c) Recovery experiment (strain cycling from 5% to 100% was carried out every 60 s). (d) Photocuring process of CNC/HAMA ink.

Fig. S16 (a) results indicate the shear-thinning property of the CNC/HAMA ink. Frequency sweep shows that the CNC/HAMA bioink is a viscoelastic material, mainly exhibiting viscous behavior at low

frequencies. The recovery experiment shows that the CNC/HAMA bioink has a certain relaxation time (10s) when the strain changes. Photocuring tests show that the CNC/HAMA ink can undergo rapid photocuring (1.1 s) under ultraviolet light irradiation, which can promptly fix the internal structure formed by the ink driven by the fluid shear force field in the experiment.

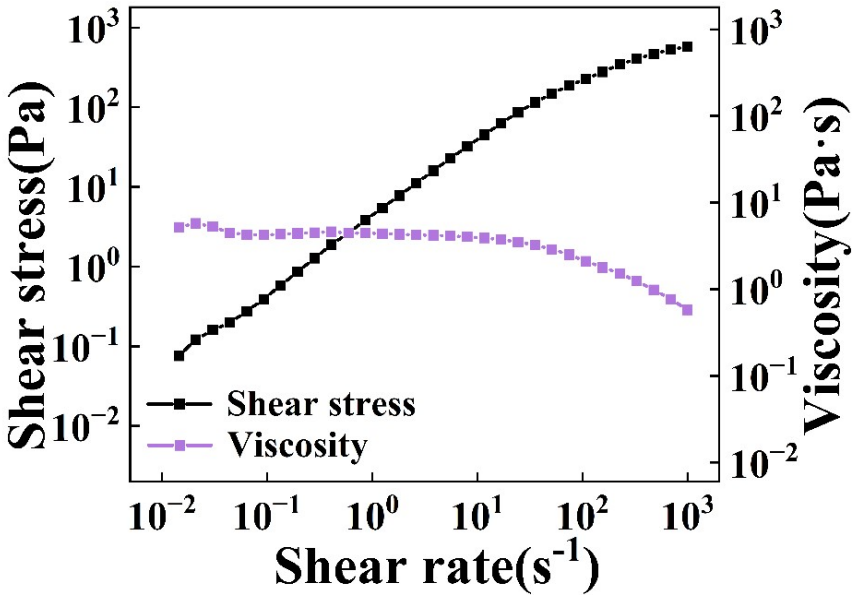

Figure S7. Shear rate-shear stress (viscosity) diagram of CNC/HAMA bioink

CNC/HAMA are aligned directionally under the action of a fluid shear force field, and in this process, the shear rate directly determines the magnitude of the shear force exerted on the molecular chains and CNC. The specific calculation process of shear rate:

For a cylindrical pipe under laminar flow conditions, the relationship between the wall shear rate, volumetric flow rate, and pipe size is expressed as:

$$\gamma = \frac{32Q}{\pi d^3} \tag{1}$$

where Q is the volumetric flow rate, and d is the pipe diameter. The CNC/HAMA ink in the manuscript is a typical shear-thinning non-Newtonian fluid (the complex viscosity decreases as the shear rate increases). The calculation of the wall shear rate for its pseudoplastic fluid model is revised as: [1, 2]

$$\gamma = \frac{3n+1}{4n} * \frac{32Q}{\pi d^3} \tag{2}$$

where n is the flow behavior index of the fluid.

According to the power-law equation:[3]

$$\tau = K * \gamma^n \quad (3)$$

the curve of shear stress and shear rate of the bioink is obtained through rheological tests. The fitting curve of shear stress and shear rate for the CNC/HAMA bioink is derived via the least squares method as:

$$log\tau = 0.580 + 0.851log\gamma \quad (4)$$

It can be known that the flow behavior index n = 0.851 (for pseudoplastic fluids, n < 1). Substituting it into the aforementioned pseudoplastic fluid model (the formula 3) gives $\gamma = 132.9\ s^{-1}$.

To exclude the influence of factors such as diffusion on orientation, we used the Reynolds number (Re) to verify the stability of the flow field, establishing a complete correlation between "fluid parameters - material response - orientation results, We calculated the Reynolds number for the perfusion process as follows:[4]

$$Re = \rho vd/\mu \quad (5)$$

where ρ is the liquid density, measured as 0.9568 g/cm³ using the pycnometer method; v is the average flow rate, with a value of $1\times10^{-7} m^3/s$; d is the inner diameter of the channel, which is 2 mm; μ is the viscosity of the ink. For the bio-ink, it is 1.84 Pa·s under the experimental conditions (temperature: 40 ℃, shear rate: $132.9\ s^{-1}$).

Under the experimental parameters, the Reynolds number calculated by Equation (5) is 0.033, which is much less than 1 (the threshold for laminar flow).[4] Dimensionless Reynolds number (Re≈0.033) confirmed laminar flow during perfusion, ruling out turbulence effects. This demonstrated that shear force is the primary driver of CNC/HAMA alignment.

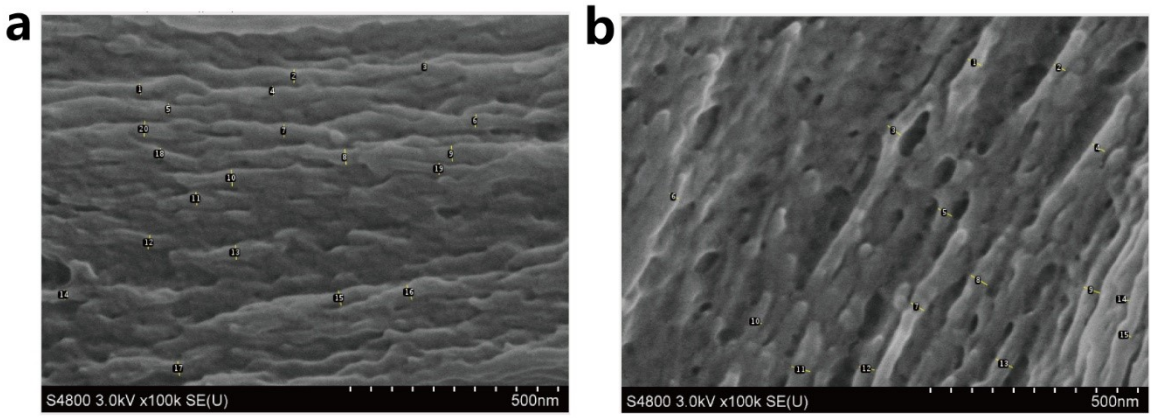

Figure S8. (a, b) Schematic diagram of the diameter of the connected fibers in the SEM spectroscopy.

Table S1. Fiber diameter statistics.

	Number	Fiber diameter (nm)	Number	Fiber diameter (nm)
Figure S8. (a)	1	35.493	11	45.245
	2	29.295	12	36.585
	3	36.907	13	44.366
	4	34.708	14	30.351
	5	36.424	15	33.905
	6	23.139		
	7	34.708		
	8	43.561		
	9	40.176		
	10	29.496		
Figure S8. (b)	1	19.861	11	29.711
	2	23.798	12	31.867
	3	29.644	13	33.655
	4	19.861	14	21.829
	5	21.829	15	34.116
	6	23.715	16	35.628
	7	29.71	17	33.829
	8	29.644	18	24.043
	9	35.628	19	23.798
	10	37.601	20	29.644

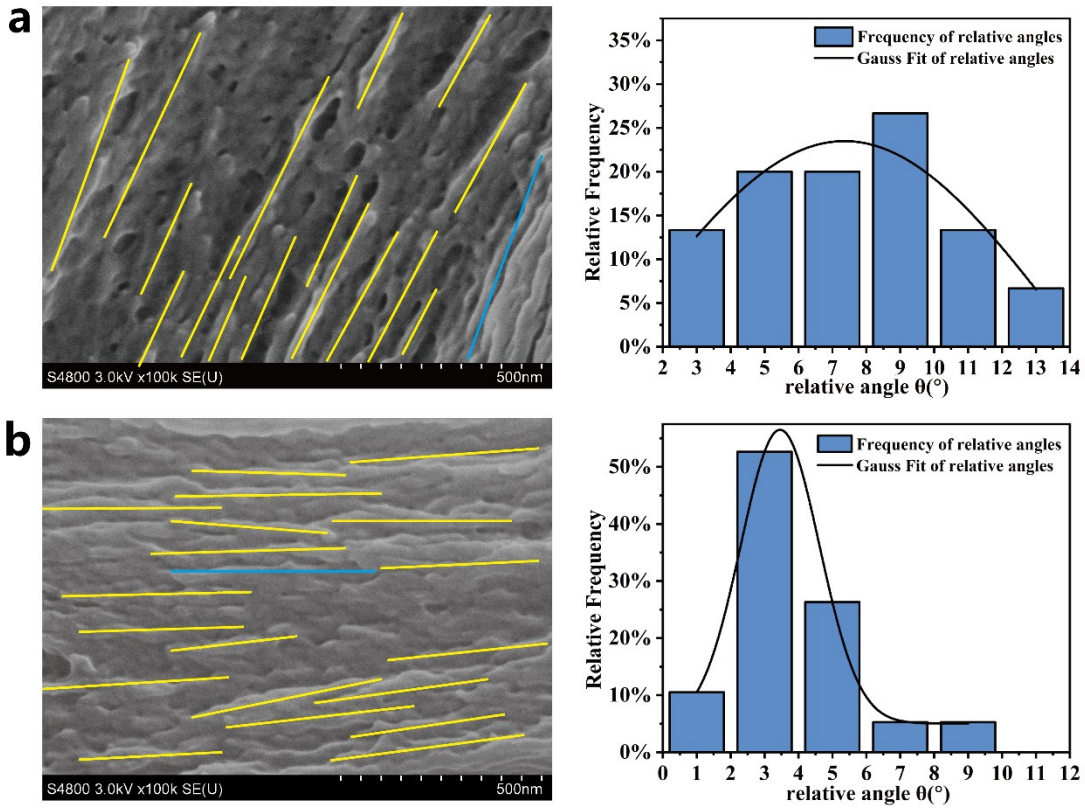

Figure S9. Calibration of CNC/HAMA composite fibers in the SEM images (The blue lines mark the reference direction, which is the direction of the fluid shear stress field. The yellow lines mark the direction of other fiber orientations.) and the frequency distribution plots of the respective corresponding orientation angles.

Based on previous literature,[5] we quantified the orientation level of CNC/HAMA composite fibers by SEM images. We defined the fibre orientation direction marked by the blue line in the figure as the reference direction (0°), and the relative angle of the orientation direction of the other fibers with respect to this fibre direction was noted as θ. The relative orientation angles of the fibers in Fig. S9 (a) and (b) were statistically calculated, and the frequency distributions were plotted in the Origin software. After data processing, their Hermans' orientation factors were calculated using the following equation:

$$f = \frac{3\langle \cos^2 \theta \rangle - 1}{2} \tag{6}$$

where <COS^{2}θ> is the statistical average value of the orientations at different angles.The f of the fibers in Fig. S9(a) is calculated to be 0.971.The f of the fibers in Fig. S9 (b) is 0.992. It can be seen that the CNC/HAMA composite fibers exhibit a high degree of anisotropy.

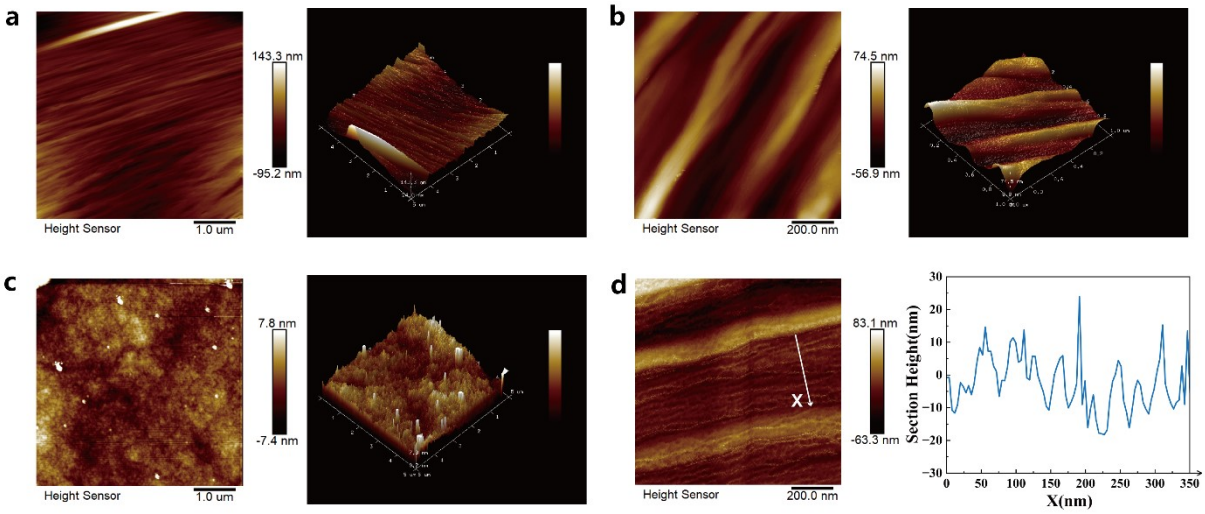

Figure S10. AFM images of pure HAMA with a fluid shear force field with a field of view of(a) 5 μm and (b)1 μm. (c) AFM image of CNC/HAMA without a fluid shear force field with a 5 μm field of view. (d) AFM image of CNC/HAMA under a fluid shear force field with a 1 μm field of view, with a schematic diagram of cross-sectional height along the X-axis (The variation of cross-sectional height along the X direction is basically consistent with the size of CNCs.).

Table S2. Significant values of Herman's orientation factor f.[6]

$\langle\cos^2\varphi\rangle$	f	Structural feature
0	-1/2	Plane normal direction is perpendicular to the reference direction
1/3	0	Isotropic distribution of plane normal direction
1	1	Plane normal direction is parallel to the reference direction

The Herman orientation factors of CNC/HAMA with applied fluid-field shear, and HAMA samples with applied fluid-field shear were calculated using the 2D-SAXS model with the taken fiber-axis direction as the reference direction.

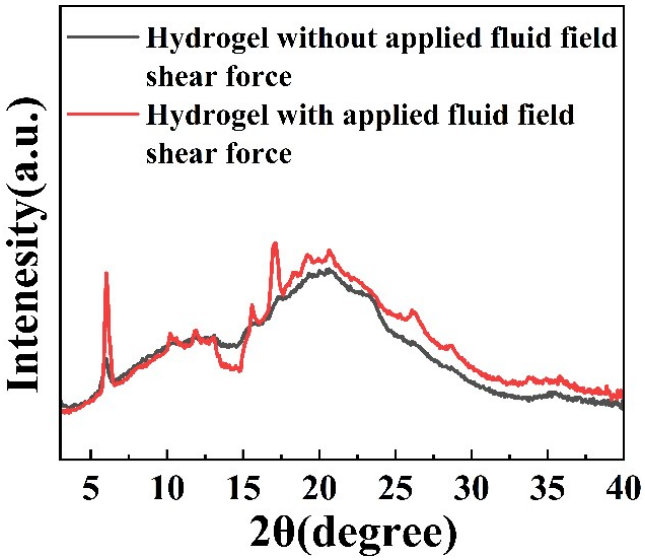

Figure S11. One-dimensional integral curves for 2D-WAXS.

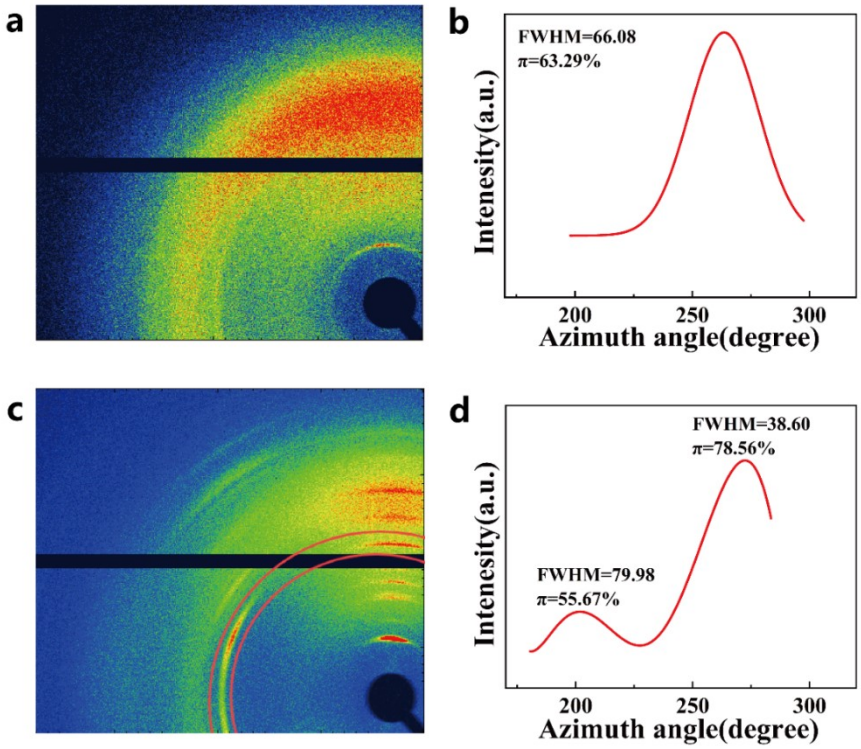

Figure S12. (a) 2D-WAXS diagram of CNC/HAMA hydrogel and (b) its azimuth integral curve at the (200) crystal plane. (c) CNC/HAMA hydrogel 2D-WAXS plot and (d) its azimuth integral curve at the location shown.

Scattering rings are not evident in Fig. S12(a) probably due to lyophilisation.

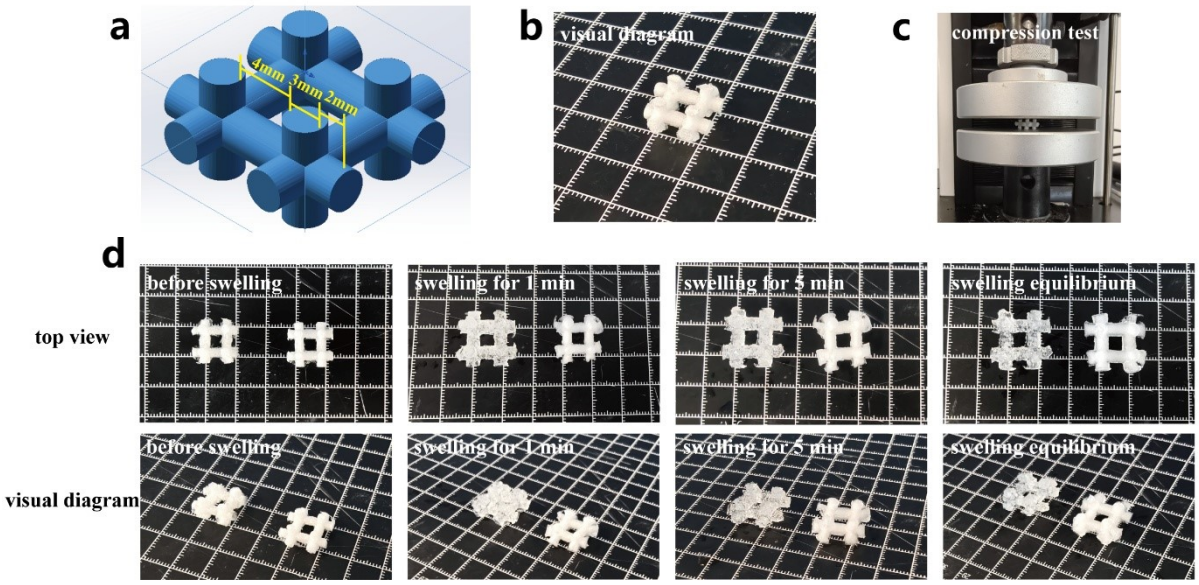

Figure S13. (a) Schematic diagram of the compressed CNC/HAMA scaffold model and (b) its physical image; (c) schematic diagram of the compression operation. (d) Swelling process of CNC/HAMA scaffolds.

Samples without applied fluid shear force field reached swelling equilibrium within 1 minute after being immersed in deionized water, showing a very obvious swelling phenomenon. In contrast, samples with applied fluid shear force field swelled relatively slowly and reached swelling equilibrium in about 5 minutes.

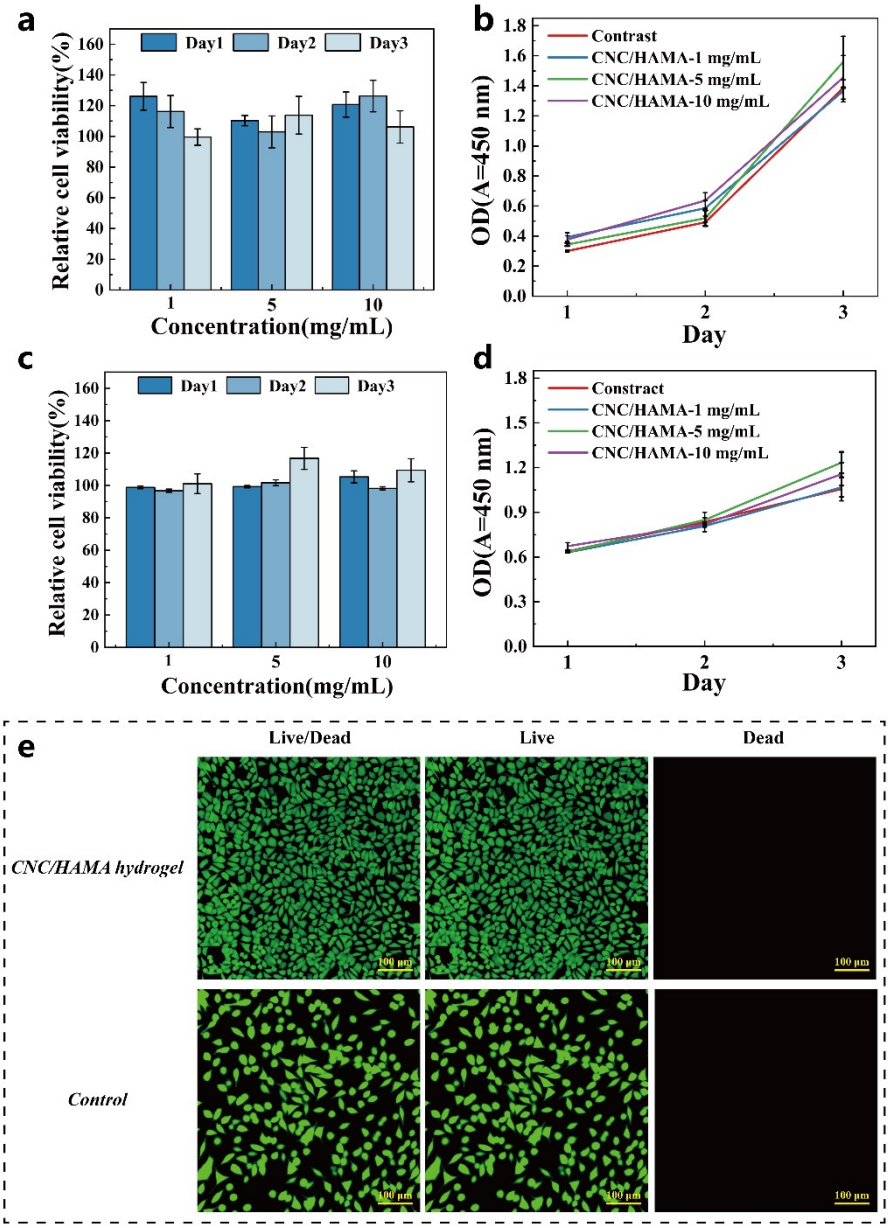

Figure S14. Cytocompatibility of the CNC/HAMA hydrogel. (a) Relative cell viability and (b) cell growth curves of L929 cells cultured in extracts of different hydrogel concentrations for 24 h, 48 h and 72 h. (c) Relative cell viability and (d) cell growth curves of MC3T3 cells cultured in extracts of different hydrogel concentrations for 24 h, 48 h and 72 h. (e) Confocal images of live/dead cell staining of L929 cells.

Live/dead staining of L929 cells directly seeded on CNC/HAMA hydrogels showed no obvious cell death compared to the control and spindle-shaped cell spreading. This confirms that the CNC/HAMA hydrogel can effectively promote cell adhesion and proliferation, meeting the application requirements for biomaterials.

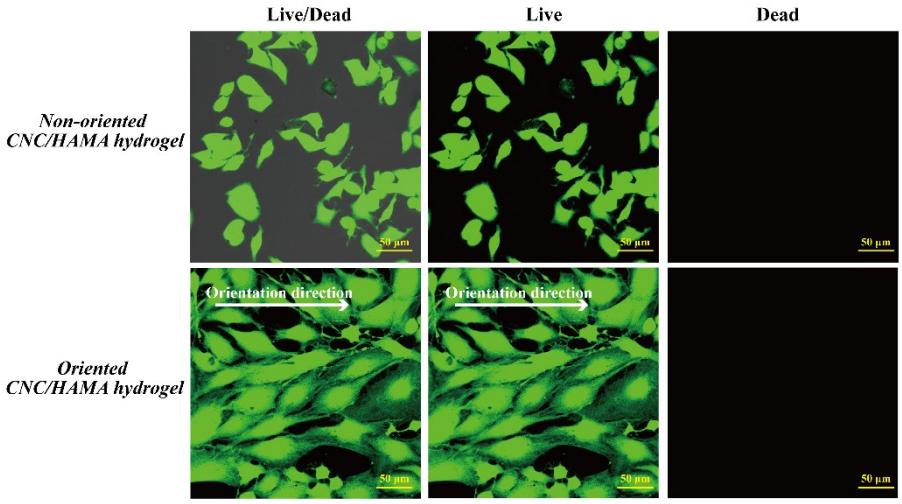

Figure S15. Confocal images of live/dead cell staining on oriented and non-oriented hydrogels after 48 hours of culture. (Orientation direction represents the alignment direction of the CNC/HAMA fibers.)

After the cells were seeded on the hydrogel matrix for 48 hours, viable cells on the oriented hydrogel exhibit a denser fluorescence signal, and MC3T3-E1 cells are distinctly aligned in an orderly fashion along the fiber orientation direction. By contrast, cells on the non-oriented hydrogel display relatively loose distribution, lacking apparent alignment patterns.

References

1. N.-D. N. Quoc-Hung Nguyen, ed., *Incompressible Non-Newtonian Fluid Flows, Continuum Mechanics - Progress in Fundamentals and Engineering Applications*, InTech, 2012.
2. P. Jaiswal, R. Shukla, D. Panda, K. D. P. Nigam and K. G. Biswas, *Chemical Engineering and Processing - Process Intensification*, 2023, 186, 109342.
3. E. Roumpea, M. Chinaud and P. Angeli, *AIChE Journal*, 2017, 63, 3599-3609.
4. S. N. A. Yusuf, Y. Asako, N. A. Che Sidik, S. B. Mohamed and W. M. A. Aziz Japar, *CFD Letters*, 2020, 12, 83-96.
5. R. A. Nargis and D. A. Jack, *Polymers*, 2023, 15, 2871.
6. C. Lang, E. C. Lloyd, K. E. Matuszewski, Y. Xu, V. Ganesan, R. Huang, M. Kumar and R. J. Hickey, *Nature Nanotechnology*, 2022, 17, 752-758.